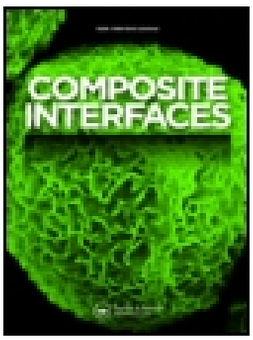

Composite Interfaces

ISSN: 0927-6440 (Print) 1568-5543 (Online) Journal homepage: http://www.tandfonline.com/loi/tcoi20

A smart coating established with encapsulation of Zinc Molybdate centred nanocontainer for active corrosion protection of mild steel: release kinetics of corrosion inhibitor

Sammit E. Karekar, Uday D. Bagale, Shirish H. Sonawane, Bharat A. Bhanvase & Dipak V. Pinjari

To cite this article: Sammit E. Karekar, Uday D. Bagale, Shirish H. Sonawane, Bharat A. Bhanvase & Dipak V. Pinjari (2018): A smart coating established with encapsulation of Zinc Molybdate centred nanocontainer for active corrosion protection of mild steel: release kinetics of corrosion inhibitor, Composite Interfaces, DOI: 10.1080/09276440.2018.1439631

To link to this article: https://doi.org/10.1080/09276440.2018.1439631

Published online: 16 Feb 2018.

COMPOSITE INTERFACES, 2018
https://doi.org/10.1080/09276440.2018.1439631

Taylor & Francis
Taylor & Francis Group

A smart coating established with encapsulation of Zinc Molybdate centred nanocontainer for active corrosion protection of mild steel: release kinetics of corrosion inhibitor

Sammit E. Karekar[a], Uday D. Bagale[c], Shirish H. Sonawane[c], Bharat A. Bhanvase[b] and Dipak V. Pinjari[a]

[a]Chemical Engineering Department, Institute of Chemical Technology, Mumbai, India; [b]Chemical Engineering Department, Laxminarayan Institute of Technology, Nagpur, India; [c]Chemical Engineering Department, National Institute of Technology, Warangal, India

ABSTRACT

In the current work smart coating of corrosion inhibitive nanocontainer was developed based on the encapsulation of ultrasonically synthesized Zinc Molybdate (ZM) nanoparticles. The ZM nanoparticles were doped ultrasonically with the layers of Myristic acid (MA), Polyaniline layer (PANI), benzotriazole layer and polyacrylic acid layer respectively to prepare layer by layer assembled nanocontainer. Results of XRD, PSD, FTIR, zeta potential and TEM analysis proves the successful formation of the layered structure of ZM nanocontainer particles. The release rate of benzotriazole at various experimental pH values was estimated using UV–vis spectroscopy. Different semi-empirical models were examined to predict the release mechanism of the benzotriazole. The corrosion inhibitive performance of ZM nanocontainers has been evaluated by incorporating 1wt % ZM nanocontainer in the epoxy based coating formulations and assessing by DC polarization measurement and Bode plots. The results from corrosion potential and Bode plots suggest the successful use of ZM nanocontainer in the multifunctional anticorrosion coating formulations.

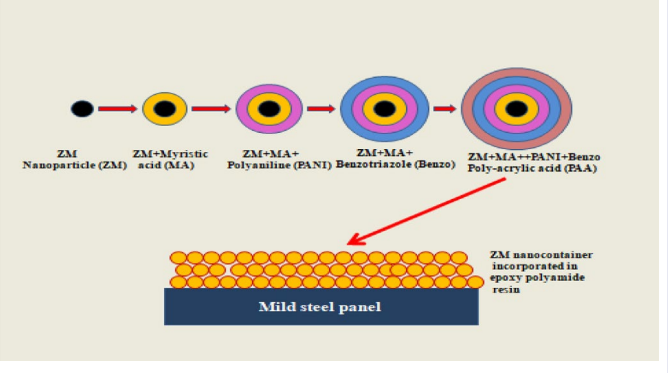

ARTICLE HISTORY
Received 18 August 2017
Accepted 12 January 2018

KEYWORDS
Ultrasonication; release kinetics; core-shell morphology; bode plots

CONTACT Bharat A. Bhanvase ba.bhanvase@nagpuruniversity.nic.in, bharatbhanvase@gmail.com; Dipak V. Pinjari dv.pinjari@ictmumbai.edu.in, dpinjari@gmail.com

1. Introduction

Corrosion is the destructive attack on the metal by a chemical or electrochemical reaction with its environment. Organic coatings are useful in protecting steel structures in corrosive environments. Since long, anticorrosive paints were formulated with lead or hexavalent chromium compounds as an active pigments [1–3]. Due to toxic nature of red lead and zinc chromates, it is being restricted due to growing environmental awareness and stringent national and international policy [4–8]. The production and paint removal of these pigments affect the environment and human health. The reduction in the use of toxic organic pigments can be accomplished by using a combination of elements such as molybdenum, phosphate, calcium, aluminum, cerium, zinc etc. Due to cationic nature of zinc, a combination of zinc with calcium, molybdenum, phosphate, or aluminum is also possible. The modified anticorrosive pigments differ in terms of their water solubility, the inhibition efficiency of the aqueous extracts and their anticorrosion action in organic coatings. Nano form of zinc molybdate has significant anticorrosive properties [9]. Nanomaterials, unlike these bulk form, have extraordinary physical and chemical properties [10,11]. Cathodic protection, anodic protection, and barrier mechanism are three useful techniques to protect the metal surface from corrosion [12,13] . Barrier technique is a preferred technique to avoid corrosion directly because it forms a layer of anticorrosive material between the metal surface and corrosive environment, thus giving low permeability of corrosive chemical to the surface of metal [14]. A corrosion inhibitor is a material that coats the metal surface, providing a protective barrier film, which in turn restricts the further corrosion. These can be incorporated into paint formulations.

The formulations in which anticorrosive liquids can be introduced into the coatings are known as Active corrosion protective formulation [15]. Direct addition of anticorrosive liquid is not preferred which affects the performance of the prepared coatings [16]. Corrosion inhibitors can be encapsulated in the layered structure of active ingredients on nanopigment core, which shows responsive release and shows better corrosion inhibiting ability compared to single corrosion inhibiting pigment [17–26] not affecting the coating performance**.** The nanocontainers which are formed by encapsulation of polyelectrolyte layer can be applicable in a variety of fields such as biomedical**,** sustained drug delivery [27], catalyst [28], textile, etc. The polyelectrolyte layer forms a matrix structure on a core material, so it can be used in various applications to release the active ingredients in a responsive manner. Formation of nanocontainer and layer by layer assembly of core corrosion inhibiting nanopigment has been put-forth by a number of researchers [20,21,23–26,29–34] in past**.**

Shchukin et al. [32] synthesized a Layer by layer (LbL) assembled nanocontainer with encapsulation of polyelectrolytes. In the layer by layer synthesis of nanocontainer, one or more layer of polyelectrolyte can be formed on the exterior of the core nanopigment / template, which offers stimuli responsive followed by controlled release. A multifunctional core and shell morphology of nanocontainer can be produced using doping of oppositely charged species on the exterior of the core substance [32]. Core and shell assembly has been reported using an emulsion method [35]. Moreover, kinetic models reported in the literature can be used to study the corrosion inhibitor release from layer-by-layer assembled nanocontainers. These existing kinetic models can indicate the corrosion inhibitor release as a function of time. The kinetic study of the corrosion inhibitor release can be used to offer information about diffusion processes and matrix degradation. The kinetic models contribute to a better

understanding of inhibitor release processes thus facilitating the optimization of existing systems and the development of new efficient systems. In many cases, for sustained release of corrosion inhibitor, theoretical equations are not available, hence in some cases more adequate empirical equations can be used.

In the present study, ZM nanoparticles were doped with three layers such as polyaniline, benzotriazole, and polyacrylic acid respectively to form shell and core assembly i.e. nanocontainer to incorporate in an alkyd resin as an active transport media against corrosion. The corrosion inhibitor (benzotriazole) is sandwiched between the two layers of polyelectrolytes i.e. first one is polyaniline and second are PAA. Polyaniline and PAA layers help in passivation, produces redox potential and results in a constant charge transfer at the metal and coating interface. Due to this mechanism, PANI is reduced from emeraldine salt form (ES) to an emeraldine base (EB) [36]. The produced shell and core assembly of nanocontainer have a competitive corrosion inhibiting effectiveness. The sustained release of corrosion inhibitor i.e. benzotriazole has been measured with the help of UV–vis spectroscopy in aqueous media at varying pH. Long lasting corrosion inhibiting ability of mild steel (MS) by using ZM nanoparticles as a core material for the synthesis of nanocontainer assembly has been confirmed along with the responsive release of benzotriazole against external environmental conditions when incorporated in alkyd resin. The available theoretical and empirical kinetic models were used to examine the release of corrosion inhibitor from ZM nanocontainers developed by Higuchi et al. [37], Hixon et al. [38], Korsmeyer et al. [39], and Hopfenberg et al. [40]. The results of different models are compared and estimation of the various kinetic parameters and validation of kinetic models has been carried out.

2. Experimental

2.1. Materials

During the synthesis of ZM nanocontainer, analytical grade sodium molybdate (Na_2MoO_4), zinc chloride ($ZnCl_2$), ammonium persulphate (APS, $(NH_4)_2S_2O_8$) as an initiator and sodium dodecyl sulfate (SDS, $NaC_{12}H_{25}SO_4$) as a surfactant were purchased from S.D. Fine Chem. and used as received without further purification. Analytical grade chemicals benzotriazole, HCl, NaOH, NaCl and ethanol procured from Thomas baker Chemicals and were used as received. Polyacrylic acid (PAA, M_w = 50 000 g mol^{-1}) procured from Sigma Aldrich and were used as received. The monomer aniline (analytical grade, M/s Fluka) was distilled two times before actual use. An epoxy resin having E.E.W. 450 g/eq, and Polyamide resin having A.V. 300 mg KOH/g were obtained from Sonal Engineering and Plastic Fabricators, Alibaug, India. Millipore water was used as a medium throughout the experimentation.

2.2. Fabrication of ZM encapsulated nanocontainers

ZM anticorrosive pigment in nano form was prepared using the ultrasonic precipitation method with the method described by Karekar et al. [9]. Initially, aqueous solutions of 10.4 M sodium molybdate and 0.98 M zinc chloride solutions were prepared separately. The solution of zinc chloride was then added dropwise to the solution of sodium molybdate under constant ultrasonic irradiation (40 kHz Sonicator (Sonics and Materials, U.S.A.) with a maximum power output of 750 W) at 40% amplitude within a time span of 10 min. The

reaction was continued for 20 min under ultrasound at room temperature (25 ± 2 °C) provided with the cooling water jacket to maintain a constant temperature. ZM nanoparticles separated from a reaction media using filtration followed by washing with water to remove dissolved impurities and then dried in an oven at 100 °C.

2.3. Fabrication of ZM encapsulated nanocontainers

Fabrication of ZM encapsulated nanocontainer was carried out according to recipe defined by Bhanvase and sonawane [17]. To make ZM encapsulated nanocontainers, previously synthesized ZM nanoparticles were used as a core material. In order to accomplish hydrophobic properties, ZM nanoparticles (5 g in 100 mL water) were surface modified with 0.5 g myristic acid solution in 10 mL methanol at 60 °C for 60 min. Surface modified ZM nanoparticles with myristic acid are expected to create negative charge onto the surface of ZM nanoparticles because of the adsorption of $C_{13}H_{27}COO^-$ functional group of the carboxylic acid. Negatively charged surface modified ZM nanoparticles were then doped with positively charged polyaniline (PANI) layer by ultrasound assisted *in situ* emulsion polymerization method to improve the strength of the adsorption of electronic charges. In that, initially, a surfactant solution was prepared by adding 3 g of SDS and 0.2 g of ZM nanoparticles in 50 mL water to wet them effectively, which was then instantaneously transferred to the sonochemical reactor (40 kHz Sonicator (Sonics and Materials, U.S.A.) with a maximum power output of 750 W). The initiator solution was prepared independently with the addition of 3.5 g APS in 20 mL of deionized water and was then added to the reactor. Five gram aniline addition was accomplished in the semi batch mode over 30 min periods. After complete addition of aniline, the reaction was allowed to proceed for next 1 h with ultrasonic irradiation and at the temperature of 4 °C. The formed product was then isolated by centrifugation (Remi Instruments Supply 220/230 V, 50 Hz, 1φ AC) at 8000 rpm (g force = 17203.2) for 10 min and later washed with deionized water to remove unreacted material and impurities. The isolated product was then dried at 60 °C in the oven for 4 h.

After formation of PANI layer, loading of corrosion inhibitor (benzotriazole) was achieved by the addition of 2 g PANI loaded ZM particles in 0.1 N NaCl solution prepared in a 100 mL deionised water. Further, deposition of positively charged corrosion inhibitor layer (benzotriazole) on the surface of PANI loaded ZM nanoparticles was carried out using 2 mg/mL of benzotriazole in ultrasound assisted environment for 20 min. Formed product was isolated by centrifugation and dried in an oven at 60 °C over 3 h and was further used for loading of PAA layer. Later in order to obtain stimuli responsive release of corrosion inhibitor, ZM nanoparticles were doped with the layer of polyacrylic acid (PAA). The adsorption of PAA layer was carried out using 2 mg/mL of PAA in 0.1 N NaCl solution with the aid of ultrasonic irradiation for 20 min. The formed product was further separated by centrifugation followed by washing with deionized water and drying in an oven at 60 °C for 48 h. The formation mechanism of ZM nanocontainer is schematically shown in Figure 1.

2.4. Preparation of nanocontainer-doped smart coatings and its application on Mild Steel (MS) panels

Preparation of nanocontainer/epoxy based smart coatings was done by incorporating the 1 wt. % of prepared nanocontainers in the epoxy resin. Incorporation of the nanocontainers in

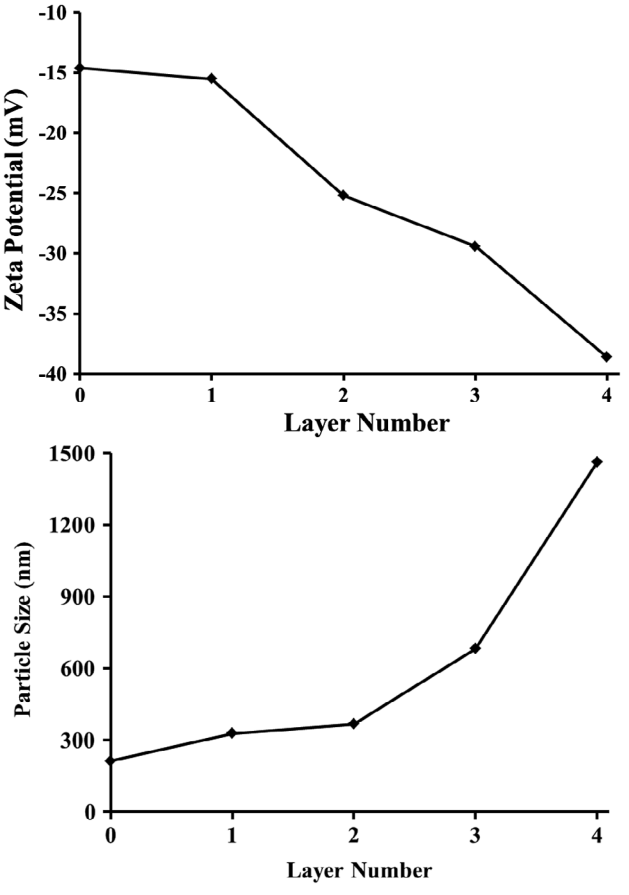

Figure 1. (a) Zeta Potential of ZM nanocontainer in water. Layer number 0: initial $ZnMoO_4$, 1: $ZnMoO_4$/PANI, 2: $ZnMoO_4$/PANI/Benzotriozole, 3: $ZnMoO_4$/PANI/Benzotriozole/PAA. (b) Growth in particle size of ZM nanocontainer. Layer number 0: initial $ZnMoO_4$, 1: $ZnMoO_4$/PANI, 2: $ZnMoO_4$/PANI/Benzotriozole, 3:$ZnMoO_4$/PANI/Benzotriozole/PAA.

epoxy resin was done by mechanical stirring for 10 min. Polyamide was selected as a curing agent, on the basis of functionality with epoxy resin the ratio of 2:1 (epoxy: polyamide) for total quantity as 10.0 g. Then above formulation was thoroughly mixed with xylene: butanol (60:40) combination to easiness the application of the coating on mild steel (MS) panels. Then, the prepared coating was applied on the sand cleaned MS panels by spray gun (nozzle diameter 1.5 mm and pressure of 4.5 bar). The panels were received from Nippon Paints India with dimension (T × W × L) of 0.5 × 100 × 150 mm. The thickness of all deposited samples was in the range of 80–90 μm. After application, the coated panels were left for curing for 7 days at ambient temperature

2.5. Characterization of the prepared ZM nanoparticles, ZM nanocontainer and its coatings

Zeta potential and particle size distribution measurements were carried out by Malvern Zetasizer Instrument (Malvern Instruments, Malvern, U.K.). The morphology of ZM

nanocontainer was performed by using transmission electron microscopy (TEM) (Technai G20 working at 200 kV). Infrared spectroscopic analysis of samples was carried out using SHIMADZU 8400S analyzer in the region of 4000–500 cm^{-1}. X-ray diffraction (XRD) pattern of ZM nanoparticles and ZM nanocontainer was recorded by using powder X-ray diffractometer (Rigaku Mini-Flox, U.S.A.). The weight loss of the sample was determined by using a thermogravimetric analysis (PerkinElmer TGA system, U.S.A.), from room temperature to 700 °C in an N_2 atmosphere at a heating rate of 10 °C/min. The UV–vis spectroscopy (SHIMADZU 160A model) was used to illustrate the self-releasing mechanism of corrosion inhibitor from ZM nanocontainers, and to fix the specific solution pH conditions to activate the corrosion inhibitor releasing.

2.5.1. Tafel plot analysis

For Tafel plot analysis, all electrochemical measurements have been performed on the computerized electrochemical analyser (supplied by Ivium Instruments, Netherlands). An MS panel was used as the working electrode with working area 1 cm^2 with a platinum sheet as the counter and a saturated calomel electrode (SCE) as the reference electrode. Polarization measurements were taken after exposure to the 0.5 M HCl, 5% NaCl and 5% NaOH solution. The potential was scanned between −2 and +2 V at a rate of 2 mV/electrochemical measurements were carried out at room temperature (30 ± 1 °C).

2.5.2. EIS measurements

The corrosion resistance of the smart coating with addition of ZM encapsulated nanocontainers was studied by EIS measurements. EIS measurements were carried out for Neat epoxy-polyamide resin coating, Epoxy with 1% nanocontainer and bare mild steel in 3.5% NaCl solution on a three-electrode cell and tested after 2 h and 24 h of immersion. Where the mild steel specimens were used as working electrode, a platinum wire as counter electrode and a saturated calomel electrode (SCE) as reference electrode. When the open circuit potential (OCP) of the mild steel specimens reached a stable value, which was recorded as a function of time, the EIS was measured at the OCP. The EIS measurement was conducted over a frequency range from 10^5 to 10^{-2} Hz. The rms width of the sinusoidal voltage signal applied to the system was 10 mV.

3. Results and discussions

3.1. Formation mechanism, zeta potential and particle size distribution of ZM nanocontainer

In formation of ZM nanocontainer initially ZM nanoparticles were synthesized by an ultrasound method according to procedure reported by Karekar et al. [9]. In order to improve the hydrophobicity of ZM nanoparticles to make it compatible with PANI, ZM nanoparticles were surface treated with Myristic acid (MA) in the presence of ultrasonic irradiations. Because of the hydrophobic nature of ZM nanoparticles and formed a negative charge on ZM nanoparticles, the adsorption of PANI layer on ZM nanoparticles was successfully established. Further, as shown in Figure 1, adsorption of the third layer of benzotriazole molecules was effectively carried out on PANI/MA/ZM particles. Finally, the deposition of the negatively charged PAA layer (fourth layer) was carried out after the successful formation

of the corrosion inhibitor layer i.e. benzotriazole layer on polyaniline (PANI) layer. Due to the application of ultrasonic irradiation, the agglomeration of ZM nanocontainer was prevented.

The Zeta potential value of surface layers is expected to change because of the changes that occur in the ionic strength of the liquids affecting the stability of the nanocontainer. Therefore, it is important to measure the zeta potential of the nanocontainer after each layer deposition. Zeta (ζ) potential after the deposition of each layer of the prepared ZM nanocontainer in water was described in Figure 1(a). The value of zeta potential of bare/uncoated ZM nanoparticles is −14.6 mV. The zeta potential after the deposition of a myristic acid layer on synthesized ZM nanoparticles was found to be −15.5 mV. This is due to adsorbed $C_{13}H_{27}COO^-$ functional group resulted from Myristic acid on the ZM nanoparticle surface. The zeta potential after the loading PANI layer was found to be –25.2 mV. It is found that the negative value of Zeta potential increases after loading PANI layer. This negative value of the Zeta potential increase is due to the occurrence of surfactant i.e. sodium dodecyl sulfate (SDS), which was used at the time of emulsion polymerization. At the time of emulsion polymerization, aniline enters into the micelle region and travels towards the head group of the micelle [41]. This causes a reduction in the value of zeta potential after loading of PANI layer. Kim et al. [42] reported that the phenyl moiety stays within the hydrophobic tail region and the polar group remain among the SDS head groups. After loading of corrosion inhibitor i.e. benzotriazole shows an abrupt increase in the negative value of zeta potential which is −29.4 mV. Finally, after adsorption of PAA layer, the zeta potential value again increases to −38.6 mV. Adsorption of PAA chains leads to an increase in this value. The zeta potential value confirms the adsorption of charged species and intra-particle interaction in the ZM nanocontainer. Gradual increase in the average size of the particle with the addition of each layer has been observed in the Figure 1(b). From the results of particle size analysis, it is established that there is a formation of the layered structure of ZM nanocontainer with a core of ZM nanoparticle. The particle size of virgin ZM nanoparticle was found to be around 214 nm and it became 329 nm after loading of the myristic acid layer. The formation of the PANI layer onto the virgin ZM nanoparticles leads to an increase in the particle size with an average value of 368 nm, the thickness of PANI layer found to be 19.5 nm. Further, after the adsorption of the benzotriazole (corrosion inhibitor), the particle size increases to 682 nm with layer thickness 157 nm, which evidently signifies that a large number of benzotriazole molecules were adsorbed on PANI loaded ZM nanoparticles. Finally, adsorption of PAA layer was established by emulsion polymerization onto the benzotriazole layer results into the average particle size of 1461 nm with an average thickness of 389.2 nm. The average particle size is found to be gradually increased after the adsorption of each layer, indicating the successful formation of ZM nanocontainer.

3.2. Morphology analysis of zinc molybdate nanocontainer

Figure 2 depicts the surface morphology of ZM nanocontainer in the form of TEM images. It clearly seems that ZM is present at core and corrosion inhibitor i.e. benzotriazole is sandwiched between the two layers of polyelectrolyte. Agglomeration of multiple particles has been observed due to the existence of electrolyte and the change in the surface charge and energy. Variation in the intensity of light around each particle clearly indicates the separate deposition of PANI/benzotriazole/PAA layers. The presence of shell and core assembly

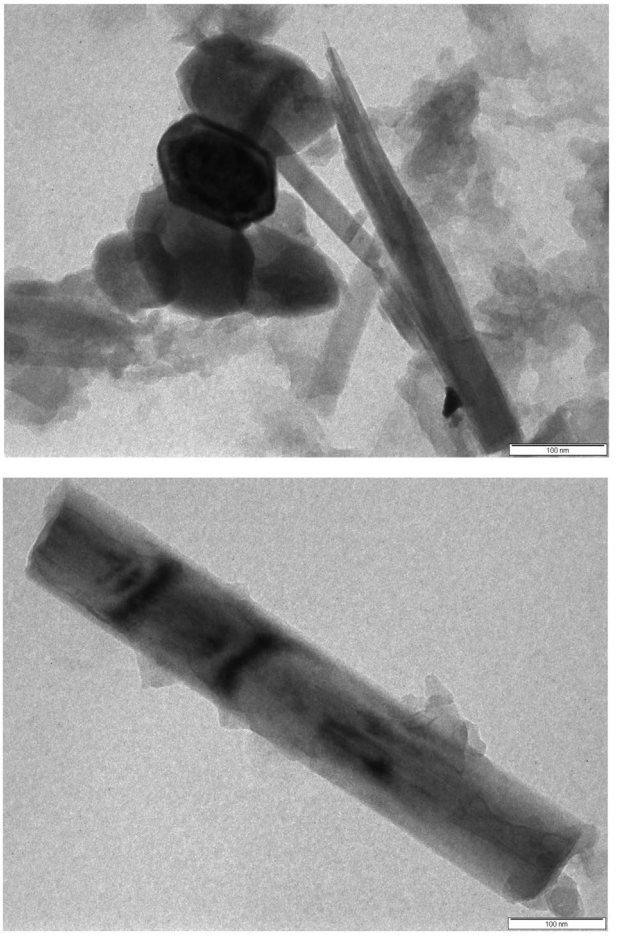

Figure 2. TEM image of ZM nanocontainers.

of ZM nanocontainer and encapsulation of organic layer on ZM nanoparticle has been established from the PSD analysis. Increase in the size of particles (Figure 1(b)) with the deposition of multiple layers confirms the presence of organic molecules. Shchukin and Mohwald [35] have described in detail the approach of coverage of particle by organic molecules and growth of particle size.

3.3. FTIR analysis of ZM encapsulated nanocontainer

Figure 3 depicts the FTIR spectrum of virgin ZM (pattern A), Surface modified ZM (pattern B), Surface modified ZM loaded with PANI (pattern C), Deposition of Benzotriazole layer on PANI loaded ZM (pattern D) and loading of PAA (Polyacrylic acid) layer on Benzotriazole loaded ZM (pattern E). FT-IR spectra of ZM nanoparticles have been shown in Figure 3 (Pattern A). At 806–950 cm^{-1} very strong Mo–O stretching vibration in $[MoO_4]^{2-}$ has been detected and at 403, 426, 462, 524 cm^{-1} weak Mo–O bending vibration was observed [43,44]. Further, ultrasound assisted synthesized ZM nanoparticles are surface modified

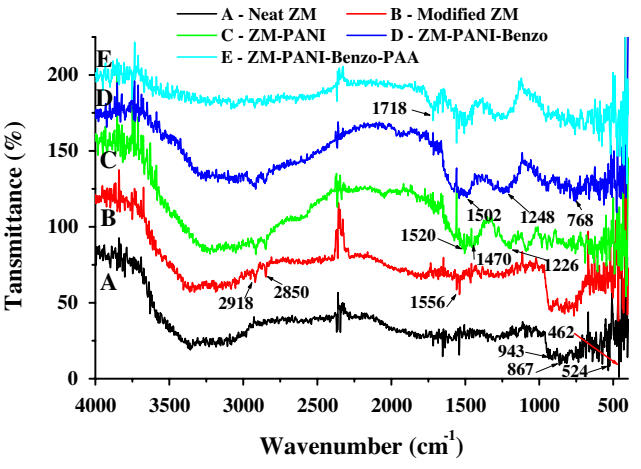

Figure 3. FTIR spectra of (A) Neat ZM (B) Modified ZM (C) ZM loaded with PANI, (D) ZM loaded with PANI and benzotriazole, (E) ZM loaded with PANI, benzotriazole and PAA (Polyacrylic acid).

with myristic acid (MA). An FTIR spectra of myristic acid modified ZM nanoparticle is depicted in Figure 3(B). In addition to the peaks of ZM, the characteristic peaks at 2918 and 2850 cm^{-1} shows stretching vibration of the C–H which arises from the $–CH_3$ and $–CH_2$ within the myristic acid respectively. The typical peak at 1556 cm^{-1} belongs to the bending of –OH. In Figure 3(C), the characteristic peak at 1226 cm^{-1} is due to (C–N) stretching mode of the amine group of PANI and the peak at 1470 cm^{-1} represents a C=C stretching mode of the quinoid rings and C=C stretching of benzenoid rings respectively [45]. Further, the characteristic peak at 1520 cm^{-1} corresponds to a secondary = N–H bending. The presence polyaniline peaks validate the creation of polyaniline on the surface of ZM nanoparticles. Figure 3(D) depicts the FTIR spectra after loading of benzotriazole on PANI loaded myristic acid surface modified ZM nanoparticles. The characteristic peak at 1502, 1248, and 758 cm^{-1} indicates uniform and even creation of layers the benzotriazole layer of PANI coated ZM. Bands which are in close proximity to the 758 cm^{-1} show benzene ring vibrations and in the vicinity of 1502 cm^{-1} the aromatic and the triazole rings stretching vibrations are observed [46]. Lastly, Figure 3(E) reflects the FTIR spectrum of ZM nanocontainer after the adsorption of PAA layer. The characteristic bands at 1718 cm^{-1} for the PAA carbonyl C=O stretching in PAA [47].

3.4. XRD analysis of ZM encapsulated nanocontainer

The XRD patterns of ZM nanoparticle and ZM nanocontainers have been shown in Figure 4. Figure 4 (pattern A) reflects the XRD graph for ZM nanoparticles. From above graph, it seems that the synthesized ZM nanoparticles are crystalline in nature [48] and belongs to the Scheelite phase [49]. The XRD peaks at 2θ value of 17.4, 25.2, 27.9, 29.1, 31.7, 34.2, 40.3, 51.8 and 52.8° belong to the planes (101), (112), (004), (114), (211), (200), (220), (312) and (224) [50]. From Debey Scherrer's formula, the crystallite size of ZM nanoparticle was estimated to be 24.9 nm at $2\theta = 27.9°$. The particle size of ZM nanoparticles estimated from XRD is similar with the PSD data reported earlier. Further due to the uncalcined state of zinc

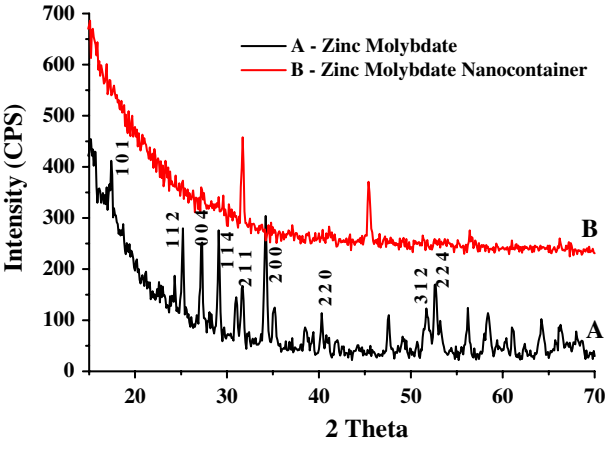

Figure 4. XRD pattern of (A) $ZnMoO_4$ nanoparticles and (B) $ZnMoO_4$ nanocontainers.

molybdate some impurity peaks of ZnO and $NaNO_3$ have been observed even after a number of hot water washing cycles. Figure 4(B) reflects the XRD pattern of ZM nanocontainer which shows that particles are completely covered with adsorbed layers of polyelectrolyte and corrosion inhibitor i.e. benzotriazole. The occurrence of XRD peaks at 27.9, 29.1, 31.7° clearly signifies the presence of zinc molybdate at the core of the nanocontainer.

3.5. Thermal stability of ZM encapsulated nanocontainer

The thermal stability of the ZM encapsulated nanocontainers are characterized by DT and TG analysis. Figure 5(a) shows the TG plot of zinc molybdate nanocontainers which shows four steps weight loss. The first weight loss (5.2 wt. %) is observed in the range of 23–170 °C (Section I) which reflects the removal of physically adsorbed and the hydrated water within the ZM nanocontainer. Secondly, the weight loss (23.7 wt. %) in between 170 and 370 °C (Section II) is observed which signifies the burning off PAA molecules. The third weight loss (17.22 wt. %) within 371 and 575 ° C (Section III) is observed which reflects the oxidative degradation of the corrosion inhibitor i.e. benzotriazole, however, which is sandwiched between the two layers of polyelectrolytes in the ZM nanocontainer core and shell assembly. This weight loss in section III clearly confirms that extra corrosion inhibitor is adsorbed in the nanocontainer. It is observed that after 575 °C (Section IV) (the fourth weight loss around 5.38 wt. %) the adsorbed PANI layer gets burned off. The weight loss from 171 to 725 °C related to the oxidative pyrolysis of hydrocarbon moieties present in the polymer. This analysis demonstrates that ZM nanocontainers are more thermally stable at higher temperatures.

Figure 5(b) shows the DT plot of ZM nanocontainers. The endothermic peak at 235 °C reflects the removal of physically adsorbed water from ZM nanocontainer [51,52]. The exothermic peaks between 235 and 650 °C signify the stepwise decomposition of PAA, PANI, and Benzotriazole (corrosion inhibitor), which have been shown by TGA analysis. Oxidative degradation of PAA, PANI and benzotriazole have been in the range of 235–650 °C [50].

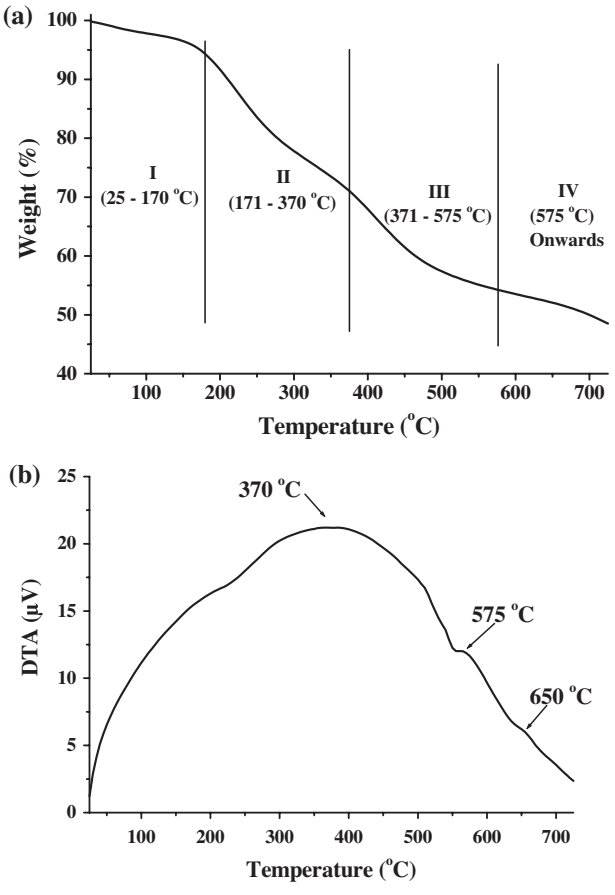

Figure 5. (a) TGA and (b) DTA analysis of $ZnMoO_4$ nanocontainer.

3.6. Measurements of self-releasing of the ZM encapsulated nanocontainer in response to solution pH

The release rate and release flux of corrosion inhibitor i.e. benzotriazole is depicted in Figure 6. While Figure 7(a) shows the swelling of the polyelectrolytes in response to pH changes to release encapsulated benzotriazole and Figure 7(b) shows the corrosion protection for steel substrate by a smart coating. It has been already reported that the benzotriazole is having good corrosion inhibiting ability for ferrous metals in the acidic environment [53–55] also in the neutral environment [56,57]. Benzotriazole leads to the formation of a passive layer on the substrate results in the lowering corrosion rate [56,57]. Study of the effect of pH of the aqueous medium (2, 4, 7 and 9) on the release and the release rate of the benzotriazole has been carried out. It is observed that the released concentration is observed to be higher with a decrease in the pH of the medium. This indicates that the release rate is more in acidic medium. The release concentration is also found to be higher with an increase in the time and then it gets stabilized. Also, the release rate of benzotriazole is found to be higher with respect to time initially and then it goes on decreasing though the concentration of benzotriazole goes on increasing in the surrounding medium but

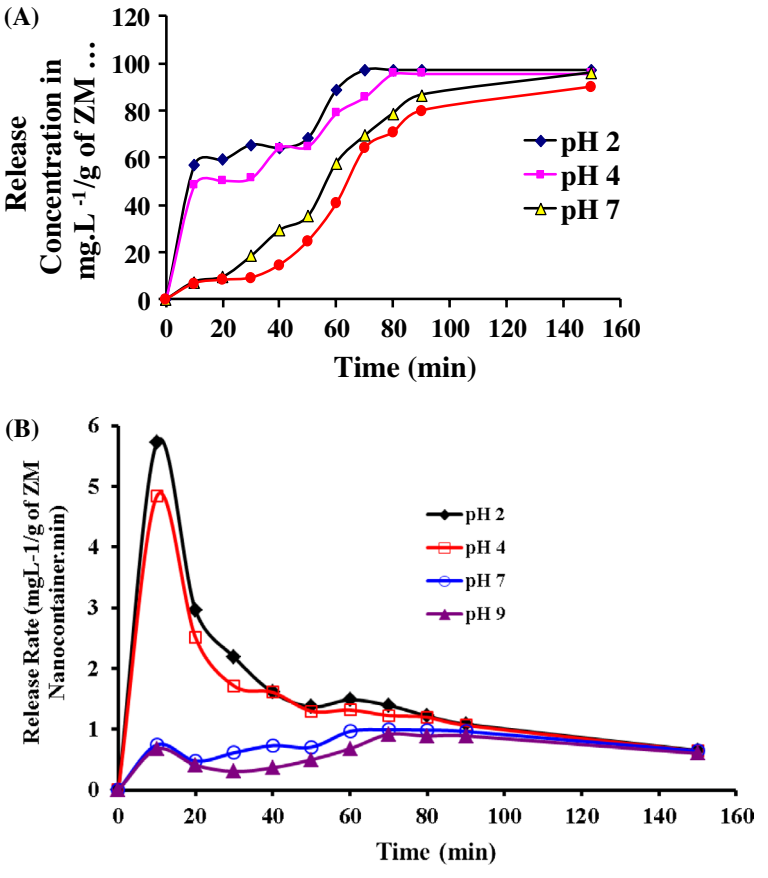

Figure 6. (A) Release rate and (B) Release flux of benzotriazole from ZM nanocontainers at different pH values.

the rate of release is lower. This increase in the concentration of released benzotriazole in the neighboring aqueous medium is responsible for the reduction in the rate of diffusion of the benzotriazole with a reduction in the concentration gradient with respect to the exposure time. Further, it is also found that the release rate and release flux are inversely proportional to the pH, indicating release rate and release flux of benzotriazole reduces with an increase in the pH value from 2 to 9. The release rate was found to reduce from 5.7 to 0.67 mgL^{-1}/g of ZM nanocontainer with an increase in the pH from 2 to 9 at the end of the 10 min. The larger release at pH 2 reflects the uniform formation of a passive layer of corrosion inhibitor i.e. benzotriazole on the surface of ferrous metal leading to corrosion inhibition in acidic medium.

Further, different kinetic models for the release of corrosion inhibitor benzotriazole have been employed to correlate the information and enhanced understanding about the release process of benzotriazole from ZM nanocontainer. The release data of corrosion inhibitor benzotriazole has been fitted to Zero order (Equation 1), first order (Equation 2), Higuchi (Equation 3), Hixson Crowell (Equation 4), Korsemeyer Peppas (Equation 5) and Hopfenberg (Equation 6) models. Various kinetic models have been used to match the benzotriazole release data for model validation.

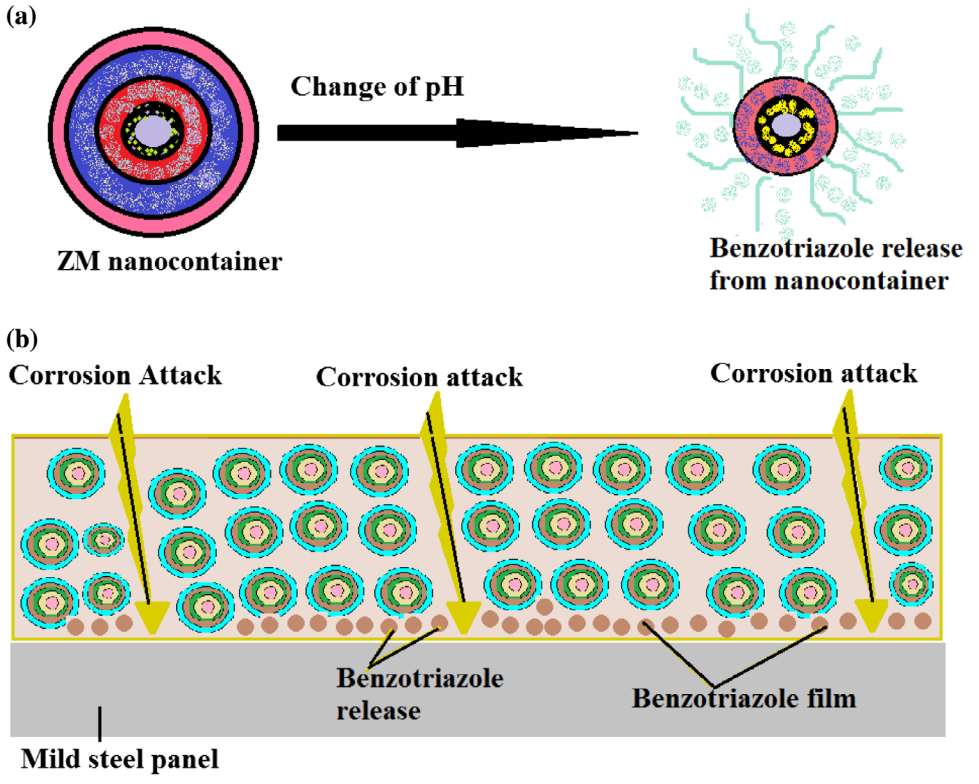

Figure 7. Schematic diagram illustrating (a) the swelling of the polyelectrolytes in response to pH changes to release encapsulated benzotriazole and (b) the principle of corrosion protection for substrate steel by a smart coating doped with inhibitor-encapsulated nanocontainers.

$$Q_t = Q_0 + k_0 t \tag{1}$$

Q_t = amount of benzotriazole released after time t, Q_0 = Initial amount of benzotriazole in the solution (in this case $Q_0 = 0$), k_0 = Zero order release constant (concentration/time) [58].

$$\ln(M_t/M_\infty) = -kt \tag{2}$$

M_t = Concentration of benzotriazole present in ZM nanocontainer at time t, M_∞ = Initial concentration of benzotriazole in ZM nanocontainer, k = First order rate constant (time^{-1}) [59] proposed by Narasimhan et al.

$$Q_t = K_H t^{1/2} \tag{3}$$

Q_t = amount of benzotriazole released after time t, K_H = Higuchi dissolution constant [37].

$$W_0^{1/3} - W_t^{1/3} = K_s t \tag{4}$$

W_t = Remaining amount of benzotriazole in ZM nanocontainer at time t, W_0 = Initial amount of benzotriazole in ZM nanocontainer, K_s = Constant incorporating the surface-volume relation [60].

$$Q_t/Q_0 = k_t t^n \tag{5}$$

Q_t = amount of benzotriazole released after time t, Q_0 = Initial amount of benzotriazole in the solution, k_t = Release rate constant, n = Release exponent [39].

$$1 - (1 - Q_t/Q_\infty)^{1/n} = k_1 t \tag{6}$$

Q_t = amount of benzotriazole released after time t, Q_∞ = amount of benzotriazole released into the solution at infinite time [40].

The release data of corrosion inhibitor benzotriazole from ZM nanocontainers at different pH values with respect to time has been fitted to zero-order (Equation 1), first-order (Equation 2), Higuchi (Equation 3), Hixson–Crowell (Equation 4), Korsemeyer– Peppas (Equation 5) and Hopfenberg (Equation 6) models. Figure 8 depicts the application of the zero order model, First order, Hixon-Crowell, Higuchi model, Korsmeyer-Peppas and Hopfenberg release model for fitting the benzotriazole release data from ZM nanocontainer. The corresponding rate constants and R^2 values are reported in Table 1. It has been further observed that the rate constant values are found to reduce with an increase in the pH value from 2 to 9 indicating that more release in the acidic region for better corrosion inhibition properties. Also, it is found that from the observed trend from Figure 8(A)–(E) and Table 1, it is found that the Korsmeyer – Peppas kinetic release model gives the better fit compared to other empirical models [38].

3.7. Corrosion resistance of the epoxy coatings doped with ZM nanocontainers

3.7.1. Electrochemical impedance spectroscopy

Figures 9(A) and 10(B) shows Bode modulus and phase angle plot obtained on the mild steel for Epoxy resin with ZM nanocontainer film, Neat Epoxy-polyamide resin film and only bare mild steel. The results shows that the impendance values were higher for Mild steel panels coated with

The results showed that the impedance values were higher for the film containing Epoxy with ZM nanocontainer at 2 h (1.63×10^5) and 24 h (1.28×10^4) of immersion in a salt solution than Neat Epoxy polyamide resin (5.69×10^2) and Bare Mild steel (6.53×10^2) at 2 h of immersion in salt solution. This result was because of both the better barrier properties, and the corrosion inhibition capacities, as reported earlier [61]. The presence of ZM nanocontainer with Epoxy resin improved the corrosion protection of the mild steel due to increase in the film thickness or dropping the porosity [62]. The shape of the phase angle plot designated the existence of single time constant. A more detailed interpretation of the EIS results can be made by numerical fitting, using the equivalent circuit depicted in Figure 10. In this equivalent circuit shown R is the resistance of the electrolyte; CP represent the capacitance of the coating, respectively.

3.7.2. Potentiodynamic polarization results

The polarization curves of the specimens, which were recorded after 1 h of immersion in the electrolyte, are illustrated in Figure 11. The corrosion current (icorr) and corrosion potential (Ecorr) were obtained using Tafel plot analysis [63]. The associated parameters (Table 2) indicate the various effects of the Zinc molybdate nanocontainer coating on the

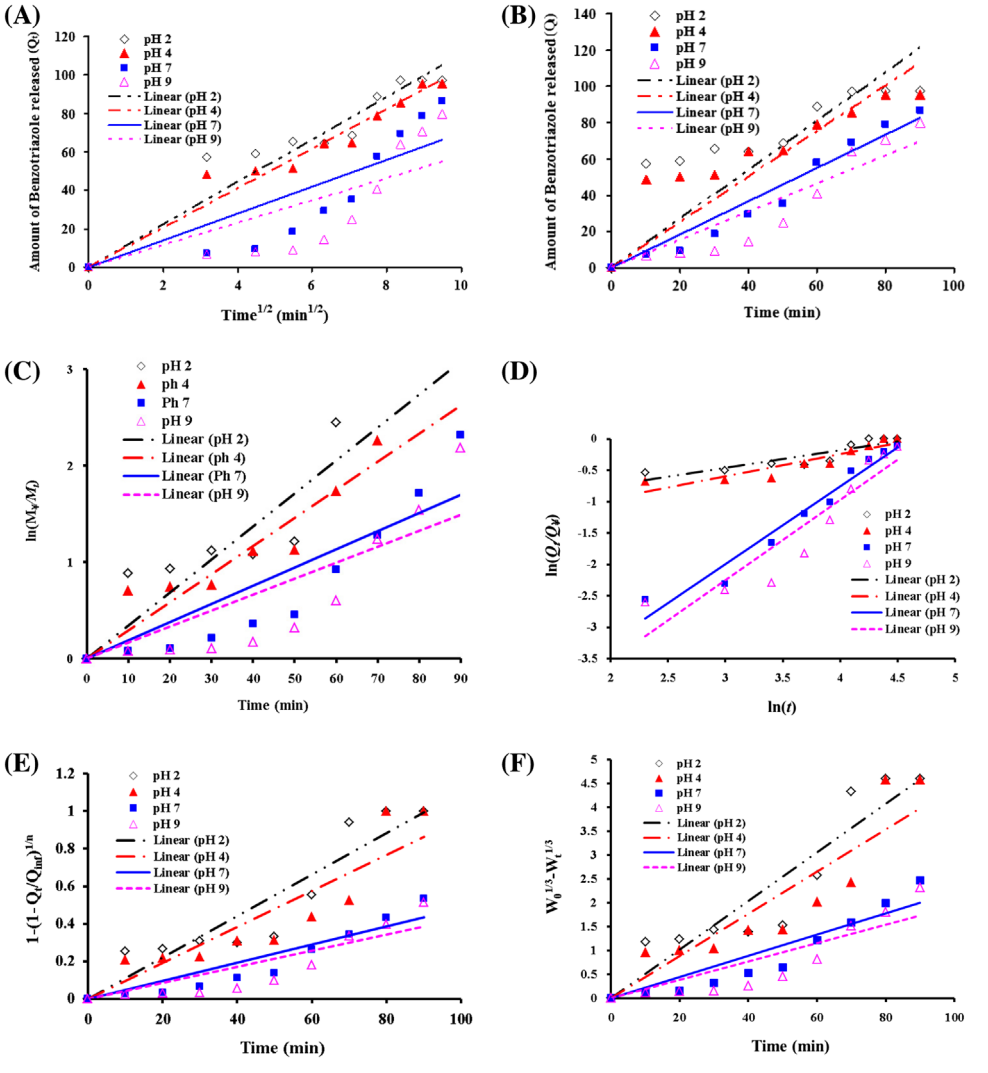

Figure 8. Release model for benzotriazole release from ZM nanocontainer at different pH (A) Higuchi model, (B) Zero Order model, (C) First Order model, (D) Korsemeyer peppas model, (E) Hopfenberg model and (E) Hixson Crowell model.

icorr, Ecorr and corrosion rate. There were noteworthy changes in the curve's features. I.e. the remarkable reduction in the cathodic current density (A/cm^2) and corrosion rate (cm/year). Degree of coating coverage on the mild steel substrate has been reproduced by Ecorr value [64]. The change in the cathodic current density reflects the inhibiting aspects of the cathodic reaction at the corrosion site, mainly the oxygen reduction reaction [64,65].

3.8. Mechanism of corrosion inhibition

It has been previously studied that the anticorrosive performance of organic compounds containing sulfur, nitrogen, oxygen, etc. is due to the establishment of the co-ordinate type

Table 1. Release kinetic data for benzotriazole release from ZM nanocontainers at different pH values.

	Zero order		First order		Hixson Crowell		Higuchi		Hopfenberg		Korsemeyer Peppas		
pH	k_0	R^2	k	R^2	K_s	R^2	K_H	R^2	K_1	R^2	k_t	R^2	n
2	1.3485	0.4334	0.0343	0.7261	0.0509	0.8763	11.099	0.8938	0.011	0.8754	0.2721	0.7924	0.2813
4	1.2583	0.6439	0.0292	0.8906	0.0441	0.8393	10.262	0.9492	0.0096	0.8368	0.1922	0.8493	0.3519
7	0.918	0.9543	0.019	0.8094	0.0222	0.874	7.010	0.7437	0.0048	0.8734	0.0033	0.9591	1.2441
9	0.7758	0.8713	0.0166	0.7298	0.0193	0.7859	5.8171	0.6313	0.0043	0.7854	0.0023	0.8621	1.2783

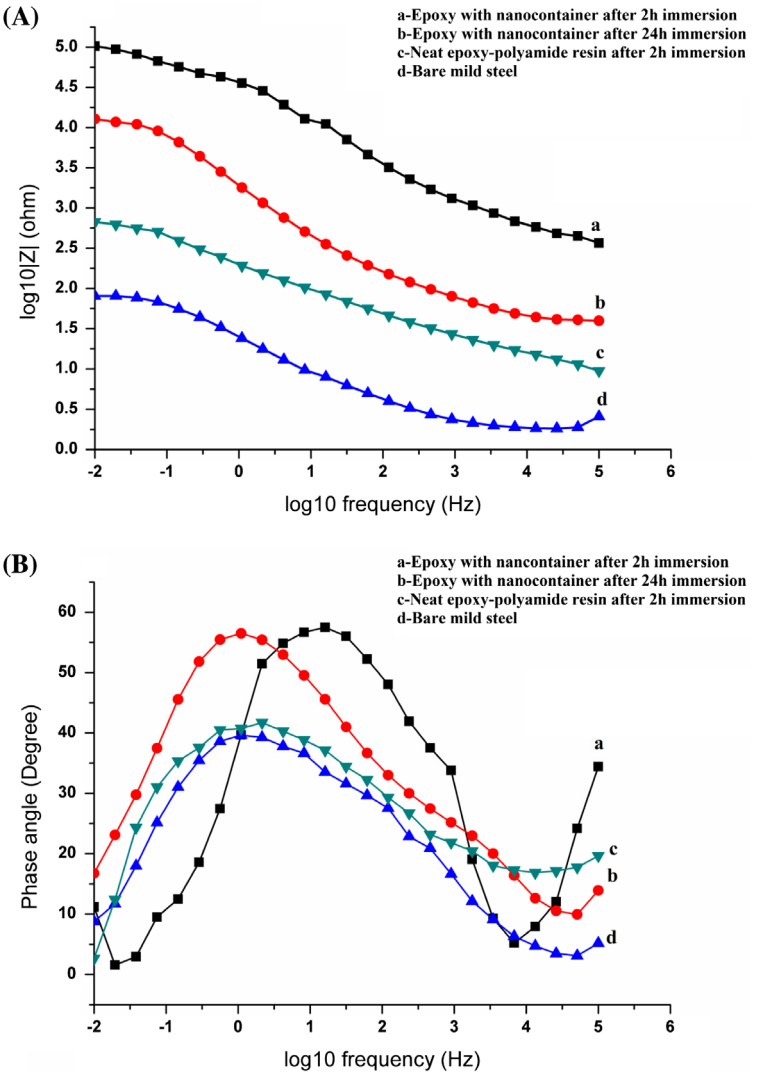

Figure 9. (A) Bode plot and (B) Phase angle plot of mild steel samples coated with neat epoxy-polyamide resin and epoxy with nanocontainers and bare mild steel at 2 h and 24 h immersion in salt solution.

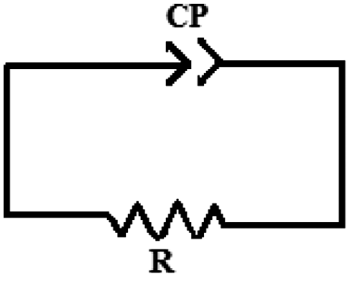

Figure 10. Equivalent circuit used for the numerical fitting of the EIS data during immersion in a 3.5% NaCl solution.

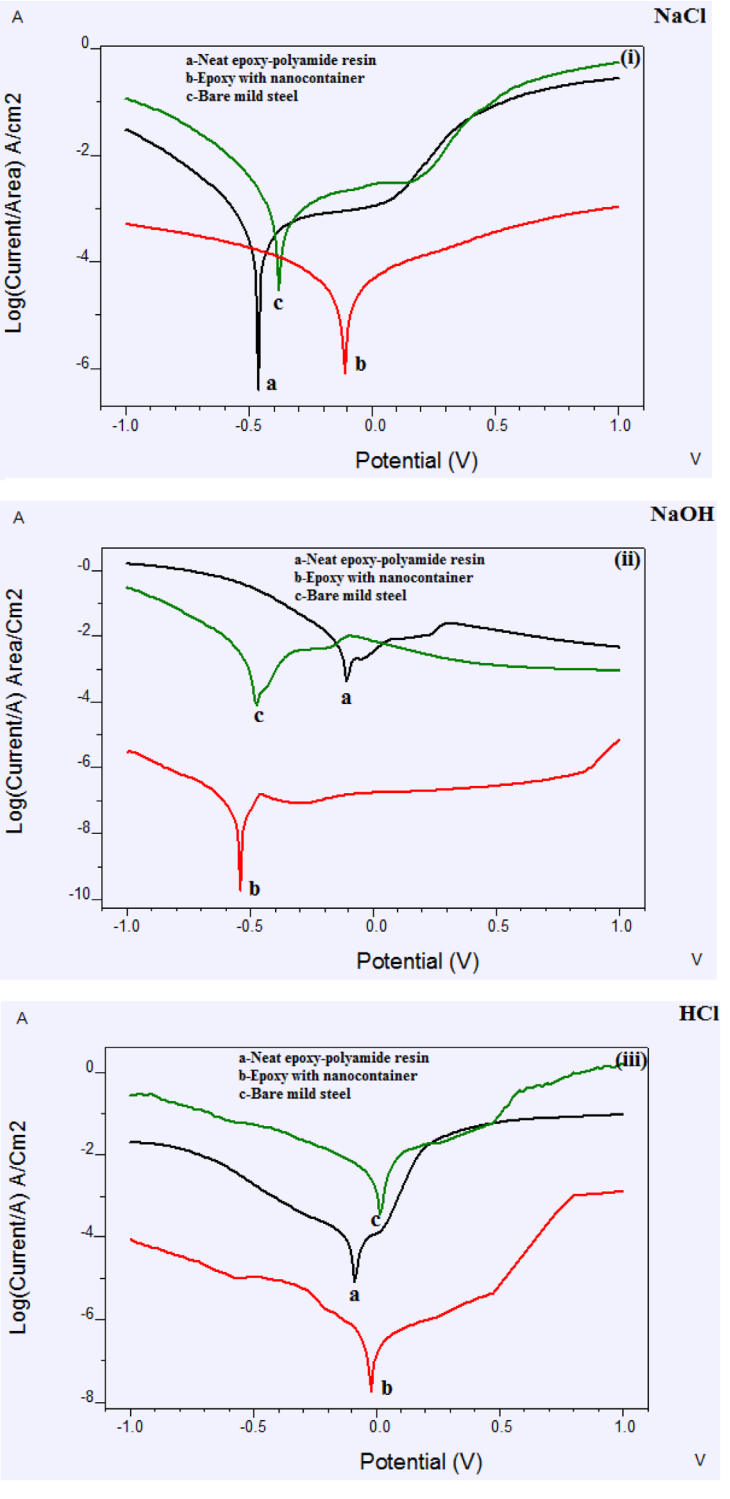

Figure 11. DC polarization measurement plot in 3 different solutions (i) 5% NaCl, (ii) 5% NaOH and (iii) 0.5 M HCl of mild steel samples coated with neat epoxy-polyamide resin and epoxy with nanocontainers and bare mild steel.

Table 2. Summary of the electrochemical parameters obtained from the polarization, measured in 0.5 M HCl, 5% NaOH and 5% NaCl solutions.

	0.5 M HCl			5% NaOH			5% NaCl		
	Bare metal	Epoxy-Polyamide	ZMN	Bare metal	Epoxy-polyamide	ZMN	Bare metal	Epoxy-polyamide	ZMN
I Corr. (A/cm^2)	0.004977	0.002529	3.471E-7	0.2248	0.04709	2.946E-9	0.0001903	5.997E-5	3.049E-5
E Corr. (v)	−0.0364	−0.6256	0.2347	−0.4306	−0.2690	−0.8178	−0.0893	−0.2434	−0.0457
Corr. Rate (mm/y)	57.77	29.36	0.004029	2611	546.9	3.42E-5	2.209	0.6961	0.354

of bond between substrate metal and lone pair of electrons in an additive. The corrosion inhibition efficiency and affinity for co-ordinate linkage can be increased by incorporating various substituents at the ring which leads to increase in effective electron density at the functional group of the additive [66–68]. In the present study benzotriazole has been used as a corrosion inhibiting compound for mild steel substrates, which is effective in acidic condition [54,69–71] as well as in a neutral condition [57]. In acidic condition benzotriaozole protects the metal from corrosion inhibition by mechanism of passivation [72,73]. Due to the passivation mechanism, corrosion inhibition of metal surface occurs by the formation of corrosion cell which leads to increase in the anticorrosive performance zinc molybdate nanoconatiner in epoxy-polyamide coating. If electrolyte cell which contains a corrosion inhibiting compound (benzotriazole) turn out to be inactive then core compound, i.e. zinc molybdate nanoparticles can protect the metal substrate from corrosion inhibition by the formation of insoluble precipitates by Zn^{2+} in salt and water, when exposed to corrosive environments. These released Zn^{2+} ions when reacts with hydroxyl ions leads to formation of passive hydroxides i.e. $Zn(OH)_2$.

$$Zn^{2+} + 2OH^{-} \rightarrow Zn(OH)_2$$

Similarly, when Zn^{2+} reacts with chloride ions forms $ZnCl_2$.

$$Zn^{2+} + 2Cl- \rightarrow ZnCl_2$$

In addition when these ions combines with molybdate ions leads to increase in the anticorrosive performance of molybdate ions [74]. Qian et al. [75] states that enhanced corrosion inhibition can be obtained with the combination of zinc and molybdate ions and which will act as a cathodic inhibitor. Above mechanism of corrosion inhibition has been supported by DC polarization test.

4. Conclusion

This study provides a successful formation of ZM nanocontainers by the encapsulation ZM nanoparticles in PANI layer and deposition of polyelectrolyte layers as well as a corrosion inhibitor (benzotriazole) in the presence of ultrasonic irradiations. TEM and SEM images provide the evidence of the formation of shell and core assembly of ZM nanocontainer. The quantitative analysis of discharge of corrosion inhibitor benzotriazole from ZM nanocontainers has been successfully performed with six different kinetic models and Korsmeyer–Peppas release model is found to be better amongst various models used to predict the release of corrosion inhibitor benzotriazole from ZM nanocontainers. The DC polarization measurement results proved that the corrosion inhibitive performance of nanocontainer based system is superior. It showed highest corrosion inhibition in 5% NaOH solution(corrosion rate 0.0005941 mm/y) compared to 0.5 M HCl (corrosion rate 0.004029 mm/y) and 5% NaCl solution (corrosion rate 0.1326 mm/y). Above results signify that the incorporation of ZM nanocontainers into paint formulation improves its corrosion inhibitive properties without terminating its consistency.

Acknowledgments

The author is thankful to Institute of Chemical Technology, Matunga, Mumbai and Department of science and technology for providing facility to carry out work and for providing sufficient funds to

purchase required equipment respectively. The author is grateful of CII, SERB and Suyog Infraspaces Pvt. Ltd. for providing sufficient financial support to carry out research work.

Disclosure statement

No potential conflict of interest was reported by the authors.

Funding

This work was supported by Department of Science and Technology, Ministry of Science and Technology; Suyog Infraspaces private limited; and Science and Engineering Research Board.

References

[1] Kendig M, Jeanjaquet S, Addison R, et al. Role of hexavalent chromium in the inhibition of corrosion of aluminum alloys. Surf Coat Tech. 2001;140:58–66.
[2] Josep VK. Paint and coating testing manual. Astm. 1995;916:1–9.
[3] Anonym. Sein und Schein. Der Spiegel; 1997.
[4] Costa M. Toxicity and carcinogenicity of Cr(VI) in animal models and humans. Crit Rev Toxicol. 1997;27:431–442.
[5] Cohen MD, Kargacin B, Klein CB, et al. Mechanisms of chromium carcinogenicity and toxicity. Crit Rev Toxicol. 1993;23:255–281.
[6] Twite RL, Bierwagen GP. Review of alternatives to chromate for corrosion protection of aluminum aerospace alloys. Prog Org Coat. 1998;33:91–100.
[7] Silbergeld EK. Implications of new data on lead toxicity for managing and preventing exposure. Environ Health Perspect. 1990;89:49–54.
[8] Bornschein RL, Hammond PB, Dietrich KN, et al. The Cincinnati prospective study of low-level lead exposure and its effects on child development: protocol and status report. Environ Res. 1985;38:4–18.
[9] Karekar SE, Bhanvase BA, Sonawane SH, et al. Synthesis of zinc molybdate and zinc phosphomolybdate nanopigments by an ultrasound assisted route: advantage over conventional method. Chem Eng Process. 2015;87:51–59.
[10] Zhao Y, Liao XH, Hong JM, et al. Synthesis of lead sulfide nanocrystals via microwave and sonochemical methods. Mater Chem Phys. 2004;87:149–153.
[11] Liao X, Chen N, Xu S, et al. A microwave assisted heating method for the preparation of copper sulfide nanorods. J Cryst Growth. 2003;252:593–598.
[12] Winston Revie R, Uhlig HH. Corrosion and corrosion control: an introduction to corrosion science and engineering. 4th ed. Hoboken (NJ): John Wiley & Sons; 2008.
[13] Roberge PR, Pierre R. Handbook of corrosion engineering library of congress cataloging-in-publication data. USA: Mac Graw-Hill; 1999.
[14] Schweitzer PA. Paint and coatings – applications and corrosion resistance. USA: CRC Press, Taylor & Francis Group; 2006.
[15] Borisova D, Mohwald H, Shchukin DG. Mesoporous silica nanoparticles for active corrosion protection. ACS Nano. 2011;5:1939–1946.
[16] Murphy EB, Wudl F. The world of smart healable materials. Prog Polym Sci. 2010;35:223–251.
[17] Sonawane SH, Bhanvase BA, Jamali AA, et al. Improved active anticorrosion coatings using layer-by-layer assembled ZnO nanocontainers with benzotriazole. Chem Eng J. 2012;189–190:464–472.
[18] Bhanvase BA, Kutbuddin Y, Borse RN, et al. Ultrasound assisted synthesis of calcium zinc phosphate pigment and its application in nanocontainer for active anticorrosion coatings. Chem. Eng. J. 2013;231:345–354.

[19] Wu DY, Meure S, Solomon D. Self-healing polymeric materials: a review of recent developments. Prog Polym Sci. 2008;33:479–522. Available from: http://linkinghub.elsevier.com/retrieve/pii/S0079670008000208.
[20] Tedim J, Poznyak SK, Kuznetsova A, et al. Enhancement of active corrosion protection via combination of inhibitor-loaded nanocontainers. ACS Appl Mater Interfaces. 2010;2:1528–1535.
[21] Zheludkevich ML, Shchukin DG, Yasakau KA, et al. Anticorrosion coatings with self-healing effect based on nanocontainers impregnated with corrosion inhibitor. Chem Mater. 2007;100:402–411.
[22] Hu Y, Chen Y, Chen Q, et al. Synthesis and stimuli-responsive properties of chitosan/poly(acrylic acid) hollow nanospheres. Polymer. 2005;46:12703–12710.
[23] Mekeridis ED, Kartsonakis IA, Pappas GS, et al. Release studies of corrosion inhibitors from cerium titanium oxide nanocontainers. J Nanopart Res. 2011;13:541–554.
[24] Zheludkevich ML, Serra R, Montemor MF, et al. Oxide nanoparticle reservoirs for storage and prolonged release of the corrosion inhibitors. Electrochem Commun. 2005;7:836–840.
[25] Suryanarayana C, Rao KC, Kumar D. Preparation and characterization of microcapsules containing linseed oil and its use in self-healing coatings. Prog Org Coat. 2008;63:72–78.
[26] Nesterova T, Dam-Johansen K, Kiil S. Synthesis of durable microcapsules for self-healing anticorrosive coatings: A comparison of selected methods. Prog Org Coat. 2011;70:342–352.
[27] Yang J, Lee J, Kang J, et al. Hollow silica nanocontainers as drug delivery vehicles. Langmuir. 2008;24:3417–3421.
[28] George C, Dorfs D, Bertoni G, et al. A cast-mold approach to iron oxide and pt/iron oxide nanocontainers and nanoparticles with a reactive concave surface. J Am Chem Soc. 2011;133:2205–2217.
[29] Kumar A, Stephenson LD, Murray JN. Self-healing coatings for steel. Prog Org Coat. 2006;55:244–253.
[30] Aramaki K. Self-healing mechanism of an organosiloxane polymer film containing sodium silicate and cerium (III) nitrate for corrosion of scratched zinc surface in 0.5 M NaCl. Corros Sci. 2002;44:1621–1632.
[31] Paliwoda-Porebska G, Stratmann M, Rohwerder M, et al. On the development of polypyrrole coatings with self-healing properties for iron corrosion protection. Corros Sci. 2005;47:3216–3233.
[32] Shchukin DG, Zheludkevich M, Yasakau K, et al. Layer-by-layer assembled nanocontainers for self-healing corrosion protection. Adv Mater. 2006;18:1672–1678.
[33] Kartsonakis IA, Kordas G. Synthesis and characterization of cerium molybdate nanocontainers and their inhibitor complexes. J Am Ceram Soc. 2010;93:65–73.
[34] Shchukin DG, Lamaka SV, Yasakau KA, et al. Active anticorrosion coatings with halloysite nanocontainers. J Phys Chem C. 2008;112:958–964.
[35] Shchukin DG, Möhwald H. Surface-engineered nanocontainers for entrapment of corrosion inhibitors. Adv Func Mater. 2007;17:1451–1458.
[36] Pereira da Silva JEP, De Torresi SIC, Torresi RM. Polyaniline acrylic coatings for corrosion inhibition: the role played by counter-ions. Corros Sci. 2005;47:811–822.
[37] Higuchi T. Mechanism of sustained-action medication. Theoretical analysis of rate of release of solid drugs dispersed in solid matrices. J Pharm Sci. 1963;52:1145–1149.
[38] Tyagi M, Bhanvase BA, Pandharipande SL. Computational studies on release of corrosion inhibitor from layer-by-layer assembled silica nanocontainer. Indus Eng Chem Res. 2014;53:9764–9771.
[39] Korsmeyer RW, Gurny R, Doelker E, et al. Mechanisms of solute release from porous hydrophilic polymers. Int J Pharm. 1983;15:25–35.
[40] Paul DR, Harris FW. Controlled Release Polymeric Formulations. ACS Symp Series Am Chem Soc Washington, DC. 1976;33:26–32.
[41] Barkade SS, Naik JB, Sonawane SH. Ultrasound assisted miniemulsion synthesis of polyaniline/Ag nanocomposite and its application for ethanol vapor sensing. Colloids Surf A. 2011;378:94–98. DOI:10.1016/j.colsurfa.2011.02.002.
[42] Kim BJ, Im SS, Oh SG. Investigation on the solubilization locus of aniline-HCl salt in SDS micelles with 1H NMR spectroscopy. Langmuir. 2001;17:565–566.

[43] Isac J, Ittyachen MA. Growth and characterization of rare-earth mixed single crystals of samarium barium molybdate. Bull Mater Sci. 1992;15:349–353.
[44] Bhattacharya S, Kar T, Bar A, et al. Structural behaviors and optical properties of semiconducting zinc–molybdate glass nanocomposites. Sci. Adv. Mater. 2011;3:284–288.
[45] Sun Y, MacDiarmid AG, Epstein AJ. Polyaniline: synthesis and characterization of pernigraniline base. J Chem Soc Chem Commun. 1990;529–531.
[46] Mennucci MM, Banczek EP, Rodrigues PRP, et al. Evaluation of benzotriazole as corrosion inhibitor for carbon steel in simulated pore solution. Cem Concr Compos. 2009;31:418–424.
[47] Lu X, Yu Y, Chen L, et al. Poly(acrylic acid)-guided synthesis of helical polyaniline microwires. Polymer. 2005;46:5329–5333.
[48] De Azevedo Marques AP, De Melo DMA, Paskocimas CA, et al. Photoluminescent BaMoO4 nanopowders prepared by complex polymerization method (CPM). J Solid State Chem. 2006;179:671–678.
[49] Ryu JH, Yoon JW, Lim CS, et al. Microwave-assisted synthesis of CaMoO4 nano-powders by a citrate complex method and its photoluminescence property. J Alloy Compd. 2005;390:245–249.
[50] Edwin Suresh Raj AM, Mallika C, Swaminathan K, et al. Zinc(II) oxide-zinc(II) molybdate composite humidity sensor. Sens Actuators B Chem. 2002;81:229–236.
[51] Takeuchi M, Martra G, Coluccia S, et al. Verification of the Photoadsorption of H 2 O molecules on TiO 2 semiconductor surfaces by vibrational absorption spectroscopy. J Phys Chem C. 2007;111:9811–9817.
[52] Yoshino K, Fukushima T, Yoneta M. Structural, optical and electrical characterization on ZnO film grown by a spray pyrolysis method. J Mater Sci. 2005;6:403–408.
[53] Matheswaran P, Ramasamy AK. Influence of benzotriazole on corrosion inhibition of mild steel in citric acid medium. E-J Chem. 2010;7:1090–1094.
[54] Selvi ST, Raman V, Rajendran N. Corrosion inhibition of mild steel by benzotriazole derivatives in acidic medium. J Appl Electrochem. 2003:1175–1182.
[55] Popova A, Christov M. Evaluation of impedance measurements on mild steel corrosion in acid media in the presence of heterocyclic compounds. Corros Sci. 2006;48:3208–3221.
[56] Cao PG, Yao JL, Zheng JW, et al. Comparative study of inhibition effects of benzotriazole for metals in neutral solutions as observed with surface-enhanced raman spectroscopy. Langmuir. 2002;18:100–104.
[57] Ramesh S, Rajeswari S. Corrosion inhibition of mild steel in neutral aqueous solution by new triazole derivatives. Electrochim Acta. 2004;49:811–820.
[58] Sciences H, Suvakanta Dash PNM, Sciences H, et al. Kinetic modeling on drug release from controlled drug delivery system. Acta Pol Pharm Drug Res. 2010;67:217–223.
[59] Narasimhan B. Mathematical models describing polymer dissolution : consequences for drug delivery. Adv Drug Deliv Rev. 2001;48:195–210.
[60] Hixson AW, Crowel1 JH. Dependence of reaction velocity upon surface and agitation. Indus Eng Chem. 1931:923–930.
[61] Zand RH, Verbeken K, et al. Evaluation of the corrosion inhibition performance of silane coatings filled with cerium salt-activated nanoparticles on hot-dip galvanized steel substrates. Int J Electrochem Sci. 2013;8:4924–4940.
[62] Montemor MF, Ferreira MGS. Analytical characterization of silane films modified with cerium activated nanoparticles and its relation with the corrosion protection of galvanised steel substrates. Prog Org Coat. 2008;63:330–337.
[63] Zhong X, Li Q, Hu J, et al. Effect of cerium concentration on microstructure, morphology and corrosion resistance of cerium – silica hybrid coatings on magnesium alloy AZ91D. Prog Org Coat. 2010;69:52–56.
[64] Sugama T. Cerium acetate-modified aminopropylsilane triol: a precursor of corrosion-preventing coating for aluminum-finned condensers. J Coat Technol Res. 2005;2:649–659.
[65] Hosseini M, et al. Corrosion protection of electro-galvanized steel by green conversion coatings. J Rare Earths. 2007;25:537–543.
[66] Granese SL, Rosales BM, et al. The inhibition action of heterocyclic nitrogen organic compounds on Fe and steel in HCl media. Corros Sci. 1992;33:1439–1453.

[67] Granese SL. Study of the inhibitory action of nitrogen-containing compounds. Corrosion. 1988;44:322–327.
[68] El SSA, Sayyah SM, El-deeb MM, et al. Poly (o-phenylenediamine) as an inhibitor of mild steel corrosion in HCl solution. Mater Chem Phys. 2010;123:20–27.
[69] Gomma G. Corrosion inhibition of steel by benzotriazole in sulphuric acid. Mater Chem Phys. 1998;55:235–240.
[70] Agrawal R, Namboodhiri TKG. The inhibition of corrosion and hydrogen embrittlement of AISI 410 stainless steel. J Appl Electrochem. 1992;22:383–389.
[71] Bentiss F, Lagrenee M, Traisnel M, et al. The corrosion inhibition of mild steel in acidic media by a new triazole derivative. Corros Sci. 1999;41:789–803.
[72] Dugdale I, Cotton J. An electrochemical investigation on the prevention of staining of copper by benzotriazole. Corros Sci. 1963;3:69–74.
[73] Poling GW. Reflection infra-red studies of films formed by benzotriazole on Cu. Corros Sci. 1970;10:359–370.
[74] Dariva CG, Galio AF. Corrosion Inhibitors – principles, mechanisms and applications. Development in Corrosion Protection. Dr. M. Aliofkhazraei (Ed.), ISBN: 978-953-51-1223-5. DOI:10.5772/57255.
[75] Qian YJ, Turgoose S. Inhibition by zinc-molybdate mixtures of corrosion of mild steel. Br Corros J. 1987;22:268–271.